24th INTERNATIONAL CONGRESS ON SOUND AND VIBRATION
23–27 July 2017, London

ICSV24
23-27JULY 2017
LONDON CALLING

EFFECTIVE BEHAVIOUR OF CORRUGATED RESONANT SURFACE EMERGING FROM NEAR-FIELD INTERACTIONS

Logan Schwan
LAUM, Université du Maine, UMR CNRS 6613, France

Olga Umnova
Acoustics Research Centre, University of Salford, U.K.
email: o.umnova@univ-salford.ac.uk

Claude Boutin
ENTPE, CeLyA, Université de Lyon, LGCB/LTDS, UMR CNRS 5513, France

The paper describes propagation of long wavelength (LW) sound in the presence of a corrugated resonant surface, that is the periodic arrangement of acoustic resonators upon a rigid panel. The method of two-scale asymptotic homogenization is applied to derive the effective boundary conditions satisfied by the LW field. The approach relies on the scale separation between the long wavelength and the characteristic size of the periodic arrangement. In that frequency range, a locally periodic boundary layer develops in the proximity of the surface. The analysis of the boundary layer is performed in order to derive to the effective boundary conditions. At the leading order, an effective surface of local reaction is found. At the corrector order, this description is supplemented by effects arising from multiple near-field interactions and the surface micro-corrugation. This leads to a non-local boundary condition that depends on the simple and double in-plane gradients of the pressure. These phenomena are illustrated for the case of 2-D periodic array of slotted cylinders with an extended neck. Effects of the centre-to-centre spacing and orientation of the resonator aperture on the non-locality and apparent end correction are studied. Results from the leading order and corrector order descriptions are compared for oblique plane wave reflection. It is shown that accounting for the corrector order terms leads to a lower resonance frequency and an additional phase shift induced by the corrugation.
Keywords: Resonant surface; Boundary layer; Two-scale asymptotic homogenisation.

1. Introduction

One of the approaches to the design of resonant metasurface for sound control is to position the resonators upon the rigid panel instead of behind it. This makes the out-of plane direction an additional degree of freedom in the design, and allows higher concentration of resonators at the surface. This, however, might lead to their close positioning and hence the possibility of strong near field interactions between the resonators and with the panel. Moreover, balancing radiation and dissipation damping for admittance matching (e.g., critical coupling for perfect sound absorption) or using several mistuned resonators per elementary cell for broadband absorption might lead to the increase of its size in relation to wavelength at resonance (poor scale separation) as often the only way to decrease visco-thermal losses or place several resonators within the unit cell is to make the cell bigger. To derive effective boundary conditions for the resonant surfaces, two-scale asymptotic homogenization has already been successfully applied [1] and it results in an effective surface admittance when only

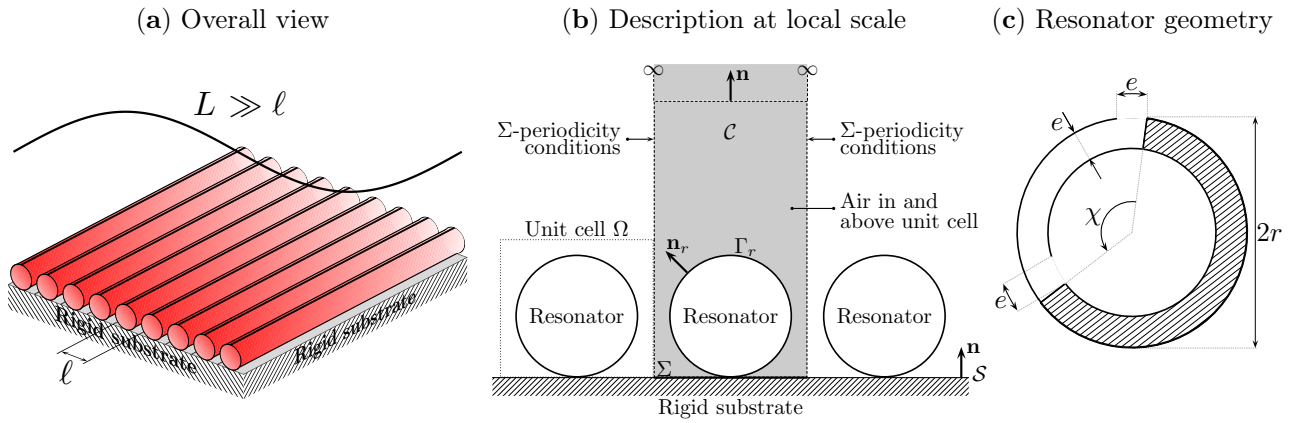

Figure 1: Example of corrugated resonant surface in 2-D. Periodic array of slotted cylinders with extended neck arranged at the rigid surface $\mathcal{S}$.

the leading order terms in expansions are accounted for. To investigate the deviation from this description in the case of the poor scale separation, the two-scale asymptotic expansions are developed up to the first corrector order to account for multiple near-field interactions between the resonators and the surface corrugation induced by their arrangement upon the rigid panel.

2. Resonant surface and boundary layer homogenization

The resonant surface consists of the 2-D Σ-periodic repetition of the unit cell Ω that includes a linear acoustic resonator (boundary Γ_r, outward unit normal vector $\mathbf{n}_r$) arranged upon the rigid plane surface $\mathcal{S}$ (normal vector $\mathbf{n}$ directed at air), with Σ being the footprint of Ω on $\mathcal{S}$, see Fig. 1. The propagation of air-borne acoustic waves, with the pressure p and the particle velocity $\mathbf{v}$, is studied in the presence of the resonant surface and under ambient conditions, with the air density ρ_e, the atmospheric pressure P_e, the adiabatic constant γ, and the sound speed $c = \sqrt{\gamma P_e/\rho_e}$ at equilibrium. The analysis is performed in the linear harmonic regime for frequencies $\omega/2\pi$ (time convention $e^{-\mathrm{i}\omega t}$) close to the natural frequency of the resonators. The fields p and $\mathbf{v}$ are governed by the equations of mass and momentum conservation:

$$\mathrm{i}\omega p = \gamma P_e \mathrm{div}(\mathbf{v}) \; ; \quad \mathrm{i}\omega\rho_e \mathbf{v} = \mathbf{grad}(p). \tag{1}$$

In response to the external field p, the resonator in the unit cell Ω produces the particle velocity $\mathbf{v}_r = \mathcal{R}(p)$ at its boundary Γ_r, where the linear operator $\mathcal{R}$ depends on the inner equilibrium of the resonator (not specified at this stage). The velocity $\mathbf{v}_r$ is balanced by the velocity $\mathbf{v}$ on the surface of the resonator, that is $\mathbf{v}\cdot\mathbf{n}_r = \mathbf{v}_r\cdot\mathbf{n}_r$ at Γ_r. At the rigid surface $\mathcal{S}$, $\mathbf{v}\cdot\mathbf{n} = 0$. We consider arrays for which a scale separation exists around the resonance, that is, the reduced wavelength $L = c/\omega$ (macroscopic scale) is much larger than the characteristic size ℓ of the unit cell Ω (microscopic scale). This condition is quantified by the small scale parameter $\epsilon = \ell/L \ll 1$ and allows application of the two-scale asymptotic homogenization [2, 3] . The homogenization procedure is based on the two-scale description of space and on the asymptotic expansions of the fields. While it is usually applied to derive the constitutive laws and effective bulk parameters of 3-D periodic media, it can also be adapted for the derivation of an equivalent boundary condition at the 2-D periodic array, by means of a boundary layer analysis [4]. To describe the phenomena at both scales, two space variables are introduced: the variable $\mathbf{x}$ of the macroscopic description (which coincides with the usual space variable), and the variable $\mathbf{y} = \epsilon^{-1}\mathbf{x}$ of the microscopic description. Differentiation is modified according to $\nabla = \nabla_{\mathbf{x}} + \epsilon^{-1}\nabla_{\mathbf{y}}$ where $\nabla_{\mathbf{x}}$ and $\nabla_{\mathbf{y}}$ are the *del* operators related to $\mathbf{x}$ and $\mathbf{y}$ respectively. Under the scale separation, the acoustic fields depend on both space variables, that is

$p(\mathbf{x},\mathbf{y})$ and $\mathbf{v}(\mathbf{x},\mathbf{y})$, and the equations of mass and momentum conservation take the form:

$$\mathrm{i}\omega p = \gamma P_e \left\{\mathrm{div}_{\mathbf{x}} + \epsilon^{-1}\mathrm{div}_{\mathbf{y}}\right\}(\mathbf{v}) \; ; \quad \mathrm{i}\omega\rho_e \mathbf{v} = \left\{\mathbf{grad}_{\mathbf{x}} + \epsilon^{-1}\mathbf{grad}_{\mathbf{y}}\right\}(p). \tag{2}$$

The micro-variations of the fields are expected to vanish some distance away from the surface, where the fields $p(\mathbf{x},\mathbf{y})$ and $\mathbf{v}(\mathbf{x},\mathbf{y})$ approach the Long-Wavelength (LW) fields $P(\mathbf{x})$ and $\mathbf{V}(\mathbf{x})$ which depend only on the macro-variable $\mathbf{x}$. From Eq. (2), it follows that:

$$\mathrm{i}\omega P(\mathbf{x}) = \gamma P_e \mathrm{div}_{\mathbf{x}}(\mathbf{V}) \; ; \quad \mathrm{i}\omega\rho_e \mathbf{V}(\mathbf{x}) = \mathbf{grad}_{\mathbf{x}}(P). \tag{3}$$

To achieve the scale transition between the LW field and the array, a Boundary Layer (BL), with the pressure $p^\star$ and the particle velocity $\mathbf{v}^\star$, is developed in the vicinity of the surface. The BL fields are superimposed upon the LW fields, that is $p = P + p^\star$ and $\mathbf{v} = \mathbf{V} + \mathbf{v}^\star$, to satisfy the locally-periodic boundary conditions and remain confined near the resonant surface. Produced by the periodic array while being forced by the LW field, the BL fields are locally Σ-periodic and modulated in the plane $\mathcal{S}$ at the macro-scale. Consequently, their dependence on the two normalised space variables is introduced in the form $p^\star(\mathbf{x}_\mathcal{S},\mathbf{y})$ and $\mathbf{v}^\star(\mathbf{x}_\mathcal{S},\mathbf{y})$, where the index $_\mathcal{S}$ denotes the projection on the plane $\mathcal{S}$. The BL fields are thus Σ-periodic and evanescent with respect to the micro-variable $\mathbf{y}$ while the first variable $\mathbf{x}_\mathcal{S}$ is used to describe the macroscopic in-plane modulation. Subtracting Eqs. (3) from Eqs. (2) and using the linearity of the problem, the BL fields $p^\star$ and $\mathbf{v}^\star$ are found to satisfy the following equations of mass and momentum conservation, where $\mathrm{div}_{\mathbf{x}}^{\mathcal{S}}$ and $\mathbf{grad}_{\mathbf{x}}^{\mathcal{S}}$ are the in-plane divergence and gradient with respect to $\mathbf{x}_\mathcal{S}$:

$$\mathrm{i}\omega p^\star(\mathbf{x}_\mathcal{S},\mathbf{y}) = \gamma P_e \left\{\mathrm{div}_{\mathbf{x}}^{\mathcal{S}} + \epsilon^{-1}\mathrm{div}_{\mathbf{y}}\right\}(\mathbf{v}^\star) \; ; \quad \mathrm{i}\omega\rho_e \mathbf{v}^\star(\mathbf{x}_\mathcal{S},\mathbf{y}) = \left\{\mathbf{grad}_{\mathbf{x}}^{\mathcal{S}} + \epsilon^{-1}\mathbf{grad}_{\mathbf{y}}\right\}(p^\star). \tag{4}$$

Note also that $\mathbf{v}_r(\mathbf{x}_\mathcal{S},\mathbf{y}) = \mathcal{R}(P(\mathbf{x}_\mathcal{S}) + p^\star(\mathbf{x}_\mathcal{S},\mathbf{y}))$, where the operator $\mathcal{R}$ depends also on the micro-variable $\mathbf{y}$. To recall that dependency, it will be denoted $\mathcal{R}_\mathbf{y}$ in the following. Then, the fields are expanded asymptotically in powers of ϵ as follows, where the order of the terms is indicated by the bracketed superscripts. For instance, $p^\star(\mathbf{x}_\mathcal{S},\mathbf{y}) = p^{\star(0)}(\mathbf{x}_\mathcal{S},\mathbf{y}) + \epsilon p^{\star(1)}(\mathbf{x}_\mathcal{S},\mathbf{y}) + \epsilon^2 \ldots$. Similar expansions are performed for $P, \mathbf{V}$, $\mathbf{v}^\star$ and $\mathbf{v}_r$. These asymptotic expansions are substituted in the governing equations and the local boundary conditions. Terms of equal powers of ϵ are collected, which results in a series of problems that can be solved successively in increasing order of powers of ϵ. At the first two orders (leading order ϵ^0 and first corrector order ϵ^1), these problem read as follows:

$$\epsilon^0 : \begin{cases} \mathrm{i}\omega\rho_e \mathbf{V}^{(0)} = \mathbf{grad}_{\mathbf{x}}\, P^{(0)}; \\ \mathrm{i}\omega P^{(0)}(\mathbf{x}) = \gamma P_e \mathrm{div}_{\mathbf{x}}(\mathbf{V}^{(0)}); \\ \mathbf{grad}_{\mathbf{y}}\, p^{\star(0)} = \mathbf{0}; \\ \mathrm{div}_{\mathbf{y}}\, \mathbf{v}^{\star(0)} = 0; \\ (\mathbf{V}^{(0)} + \mathbf{v}^{\star(0)}) \cdot \mathbf{n} = 0 \text{ at } \Sigma; \\ (\mathbf{V}^{(0)} + \mathbf{v}^{\star(0)}) \cdot \mathbf{n}_r = \mathbf{v}_r^{(0)} \cdot \mathbf{n}_r \text{ at } \Gamma_r; \\ \mathbf{v}_r^{(0)} = \mathcal{R}_\mathbf{y}\left(P^{(0)} + p^{\star(0)}\right) \text{ at } \Gamma_r; \\ \mathbf{v}^{\star(0)} \to \mathbf{0} \text{ as } \mathbf{y}\cdot\mathbf{n} \to \infty; \\ p^{\star(0)} \to 0 \text{ as } \mathbf{y}\cdot\mathbf{n} \to \infty; \\ \mathbf{v}^{\star(0)} \text{ and } p^{\star(0)} \; \Sigma\text{-periodic with } \mathbf{y}_\mathcal{S}; \end{cases} \quad ; \quad \epsilon^1 : \begin{cases} \mathrm{i}\omega\rho_e \mathbf{V}^{(1)} = \mathbf{grad}_{\mathbf{x}}\, P^{(1)}; \\ \mathrm{i}\omega P^{(1)}(\mathbf{x}) = \gamma P_e \mathrm{div}_{\mathbf{x}}(\mathbf{V}^{(1)}); \\ \mathrm{i}\omega\rho_e \mathbf{v}^{\star(0)} = \mathbf{grad}_{\mathbf{y}}\, p^{\star(1)}; \\ \mathrm{div}_{\mathbf{y}}\, \mathbf{v}^{\star(1)} + \mathrm{div}_{\mathbf{x}}^{\mathcal{S}}\, \mathbf{v}^{\star(0)} = 0; \\ (\mathbf{V}^{(1)} + \mathbf{v}^{\star(1)}) \cdot \mathbf{n} = 0 \text{ at } \Sigma; \\ (\mathbf{V}^{(1)} + \mathbf{v}^{\star(1)}) \cdot \mathbf{n}_r = \mathbf{v}_r^{(1)} \cdot \mathbf{n}_r \text{ at } \Gamma_r; \\ \mathbf{v}_r^{(1)} = \mathcal{R}_\mathbf{y}\left(P^{(1)} + p^{\star(1)}\right) \text{ at } \Gamma_r; \\ \mathbf{v}^{\star(1)} \to \mathbf{0} \text{ as } \mathbf{y}\cdot\mathbf{n} \to \infty; \\ p^{\star(1)} \to 0 \text{ as } \mathbf{y}\cdot\mathbf{n} \to \infty; \\ \mathbf{v}^{\star(1)} \text{ and } p^{\star(1)} \; \Sigma\text{-periodic with } \mathbf{y}_\mathcal{S}; \end{cases} \tag{5}$$

3. Macroscopic description up to the first corrector order

The problem described by Eq. (5) is now solved. First, the BL quasi-static equilibrium $\mathbf{grad}_\mathbf{y}\, p^{\star(0)} = \mathbf{0}$ combined with its evanescence leads to $p^{\star(0)} = 0$, that is the pressure is purely macroscopic at the leading order. Then, the integration of the equations $\mathrm{div}_\mathbf{y}\, \mathbf{v}^{\star(0)} = 0$ and $\mathrm{div}_\mathbf{y}\, \mathbf{V}^{(0)}(\mathbf{x}) = 0$ of local

incompressibility over the column $\mathcal{C}$ of air inside and above the unit cell (see Fig. 1(b)), leads to the following relations when accounting for the periodicity and BL evanescence:

$$\int_\Gamma \mathbf{v}^{\star(0)} \cdot \mathbf{n}_\Gamma \, d\Gamma_\mathbf{y} = 0 \quad ; \quad \int_\Gamma \mathbf{V}^{(0)} \cdot \mathbf{n}_\Gamma \, d\Gamma_\mathbf{y} = |\Sigma|_\mathbf{y} \, \mathbf{V}^{(0)} \cdot \mathbf{n}; \tag{6}$$

where $\Gamma = \Sigma \cup \Gamma_r$, with $\mathbf{n}_\Gamma = \mathbf{n}_r$ at Γ_r and $\mathbf{n}_\Gamma = \mathbf{n}$ at Σ; and $|\Sigma|_\mathbf{y} = \int_\Sigma d\Sigma_\mathbf{y}$ is the $\mathbf{y}$-integrated surface area of the 2-D period Σ. Combining Eq. (6) with the integration of the local boundary conditions over Γ leads to the following condition at $\mathcal{S}$:

$$\mathbf{V}^{(0)} \cdot \mathbf{n} = \frac{Q^{(0)}}{|\Sigma|_\mathbf{y}} \; ; \;\; Q^{(0)} = \int_{\Gamma_r} \mathbf{v}_r^{(0)} \cdot \mathbf{n}_r \, d\Gamma_\mathbf{y} = Y P^{(0)} \; ; \;\; Y = \int_{\Gamma_r} \mathcal{R}_\mathbf{y}(1) \cdot \mathbf{n}_r \, d\Gamma_\mathbf{y}; \tag{7}$$

where $Q^{(0)}$ and Y are the $\mathbf{y}$-integrated acoustic flux and admittance produced by the resonator in the unit cell. Equation (7) thus leads to the boundary condition $\mathbf{V}^{(0)} \cdot \mathbf{n} = -\Upsilon P^{(0)}$ at $\mathcal{S}$ with the effective surface admittance $\Upsilon = -Y/|\Sigma|_\mathbf{y}$. This leading order approximation agrees well with the measurements when the scale separation is sharp [1]. To investigate the deviation from this description in the case of the poor scale separation, the corrector order terms need to be considered. Using equations from the leading order description, supplemented by the momentum conservation $\mathrm{i}\omega\rho_e \mathbf{v}^{\star(0)} = \mathbf{grad}_\mathbf{y} \, p^{\star(1)}$, the BL pressure $p^{\star(1)}$ can be solved for. Since $\mathbf{V}^{(0)} = -\Upsilon P^{(0)}\mathbf{n} + \mathbf{grad}_\mathbf{x}^\mathcal{S} P^{(0)}/\mathrm{i}\omega\rho_e$ in the unit cell Ω, the boundary condition at Γ_r in Eq. (7) becomes:

$$\mathbf{n}_r \cdot \mathbf{grad}_\mathbf{y} \, p^{\star(1)} = \mathbf{n}_r \cdot \left[\rho_e c \mathcal{R}_\mathbf{y}(1) + \rho_e c \Upsilon \mathbf{n}\right] \mathrm{i}\omega P^{(0)}/c - \mathbf{n}_r \cdot \mathbf{grad}_\mathbf{x}^\mathcal{S} P^{(0)} \quad \text{at } \Gamma_r \tag{8}$$

while $\mathbf{n} \cdot \mathbf{grad}_\mathbf{y} \, p^{\star(1)} = 0$ at $\mathcal{S}$. Consequently, the pressure $p^{\star(1)}$ is linearly forced by $\mathrm{i}\omega P^{(0)}/c$ and $\mathbf{grad}_\mathbf{x}^\mathcal{S} P^{(0)}$ and can be written in the form:

$$p^{\star(1)}(\mathbf{x}_\mathcal{S}, \mathbf{y}) = -\mathrm{i}\omega a^{(1)}(\mathbf{y}) P^{(0)}(\mathbf{x}_\mathcal{S})/c - \mathbf{b}_\mathcal{S}^{(1)}(\mathbf{y}) \cdot \mathbf{grad}_\mathbf{x}^\mathcal{S} P^{(0)} \tag{9}$$

where the scalar field $a^{(1)}(\mathbf{y})$ and the vector field $\mathbf{b}_\mathcal{S}^{(1)}(\mathbf{y})$, with the components $b_{i\in\{1,2\}}^{(1)}$ in the in-plane directions $\mathbf{e}_{i\in\{1,2\}}$, are the elementary solutions of the following cell problems:

$$\left\{ \begin{array}{l} \mathrm{div}_\mathbf{y} \left[\mathbf{grad}_\mathbf{y} \, a^{(1)}\right] = 0; \\ \mathbf{grad}_\mathbf{y} \, a^{(1)} \cdot \mathbf{n}_r = -\rho_e c \left[\mathcal{R}_\mathbf{y}(1) + \Upsilon \mathbf{n}\right] \cdot \mathbf{n}_r \text{ at } \Gamma_r; \\ \mathbf{grad}_\mathbf{y} \, a^{(1)} \cdot \mathbf{n} = -\rho_e c \Upsilon \text{ at } \Sigma; \\ \mathbf{grad}_\mathbf{y} \, a^{(1)} \to \mathbf{0} \text{ as } \mathbf{y} \cdot \mathbf{n} \to \infty; \\ a^{(1)} \to 0 \text{ as } \mathbf{y} \cdot \mathbf{n} \to \infty; \\ a^{(1)} \quad \Sigma\text{-periodic with } \mathbf{y}_\mathcal{S}. \end{array} \right. ; \left\{ \begin{array}{l} \mathrm{div}_\mathbf{y} \left[\mathbf{grad}_\mathbf{y} \, b_i^{(1)} - \mathbf{e}_i\right] = 0; \\ \left[\mathbf{grad}_\mathbf{y} \, b_i^{(1)} - \mathbf{e}_i\right] \cdot \mathbf{n}_\Gamma = 0 \text{ at } \Gamma; \\ \mathbf{grad}_\mathbf{y} \, b_i^{(1)} \to \mathbf{0} \;\; \text{as } \mathbf{y} \cdot \mathbf{n} \to \infty; \\ b_i^{(1)} \to 0 \quad \text{as } \mathbf{y} \cdot \mathbf{n} \to \infty; \\ b_i^{(1)} \quad \Sigma\text{-periodic with } \mathbf{y}_\mathcal{S}. \end{array} \right. \tag{10}$$

The BL field $-\mathrm{i}\omega a^{(1)}/c$ is radiated by the resonators in response to the unit LW pressure $P^{(0)} \equiv 1$ while $\mathbf{b}_\mathcal{S}^{(1)}$ is related to the micro-corrugation of the surface. $a^{(1)}$ depends on frequency due to the frequency dependent response function $\mathcal{R}_\mathbf{y}$ while $\mathbf{b}_\mathcal{S}^{(1)}$ is purely geometrical. Equations for $\mathbf{b}^{(1)}$ are somewhat similar to those of the cell problems in homogenisation of periodic porous media [5]. Further, the weak formulation of Eqs. (10) over the column $\mathcal{C}$ of air inside and above the unit cell with $\hat{p}$ as the test-field reads:

$$\mathcal{F}_\mathbf{y}(a^{(1)}, \hat{p}) = \int_\Gamma \rho_e c \hat{p} \left[\mathcal{R}_\mathbf{y}(1) + \Upsilon \mathbf{n}\right] \cdot \mathbf{n}_\Gamma \, d\Gamma_\mathbf{y} \quad ; \qquad \mathcal{F}_\mathbf{y}(b_i^{(1)}, \hat{p}) = -\int_\Gamma \hat{p} \mathbf{n}_\Gamma \cdot \mathbf{e}_i \, d\Gamma_\mathbf{y} \tag{11}$$

where $\mathcal{F}_\mathbf{y}(p, \hat{p}) = \int_\Gamma \mathbf{grad}_\mathbf{y} p \cdot \mathbf{grad}_\mathbf{y} \hat{p} \, d\Gamma_\mathbf{y}$. Now, integrating the equation $\mathrm{div}_\mathbf{y} \, \mathbf{v}^{\star(1)} + \mathrm{div}_\mathbf{x}^\mathcal{S} \, \mathbf{v}^{\star(0)} = 0$ of mass conservation over the column $\mathcal{C}$, accounting for the BL periodicity and evanescence, and the local boundary conditions at Γ, the following equation is derived:

$$\frac{1}{|\Sigma|_\mathbf{y}} \int_\Gamma \mathbf{v}^{\star(1)} \cdot \mathbf{n}_\Gamma \, d\Gamma_\mathbf{y} = -\frac{\mathbf{A}_\mathcal{S}^{(1)}}{\rho_e c} \cdot \mathbf{grad}_\mathbf{x}^\mathcal{S} P - \frac{\mathbb{B}_\mathcal{S}^{(1)}}{\mathrm{i}\omega\rho_e} : \mathbf{grad}_\mathbf{x}^\mathcal{S} \left[\mathbf{grad}_\mathbf{x}^\mathcal{S} P^{(0)}\right] \tag{12}$$

where : is the double contraction and the in-plane vector $\mathbf{A}_{\mathcal{S}}^{(1)}$ and tensor $\mathbb{B}_{\mathcal{S}}^{(1)}$ are defined as follows:

$$\mathbf{A}_{\mathcal{S}}^{(1)}|_{i\in\{1,2\}} = \frac{-1}{|\Sigma|_{\mathbf{y}}}\int_{\Gamma} a^{(1)}\mathbf{n}_{\Gamma}\cdot\mathbf{e}_i\, d\Gamma_{\mathbf{y}} \quad ; \qquad \mathbb{B}_{\mathcal{S}}^{(1)}|_{i,j\in\{1,2\}} = \frac{-1}{|\Sigma|_{\mathbf{y}}}\int_{\Gamma} b_i^{(1)}\mathbf{n}_{\Gamma}\cdot\mathbf{e}_j\, d\Gamma_{\mathbf{y}}. \tag{13}$$

Using Eq. (11) with $a^{(1)}$ or $b_i^{(1)}$ as the test-fields, the following relations are found:

$$\mathbf{A}_{\mathcal{S}}^{(1)}|_i = \frac{\mathcal{F}_{\mathbf{y}}(b_i^{(1)}, a^{(1)})}{|\Sigma|_{\mathbf{y}}} = \int_{\Gamma}\frac{\rho_e c b_i^{(1)}}{|\Sigma|_{\mathbf{y}}}\left[\mathcal{R}_{\mathbf{y}}\left(1\right) + \Upsilon\mathbf{n}\right]\cdot\mathbf{n}_{\Gamma}\, d\Gamma_{\mathbf{y}}\ ;\ \ \mathbb{B}_{\mathcal{S}}^{(1)}|_{ij} = \frac{\mathcal{F}_{\mathbf{y}}(b_i^{(1)}, b_j^{(1)})}{|\Sigma|_{\mathbf{y}}}. \tag{14}$$

While the first relation establishes a link between the fields $a^{(1)}$ and $b_i^{(1)}$, the expression for $\mathbb{B}_{\mathcal{S}}^{(1)}|_{ij}$ shows that the matrix $\mathbb{B}_{\mathcal{S}}^{(1)}$ is symmetric positive. The flux $Q^{(1)}$ produced by the resonator in the cell Ω per unit surface of the 2-D period Σ is:

$$\frac{Q^{(1)}}{|\Sigma|_{\mathbf{y}}} = \frac{1}{|\Sigma|_{\mathbf{y}}}\int_{\Gamma_r}\mathbf{v}_r^{(1)}\cdot\mathbf{n}_r\, d\Gamma_{\mathbf{y}} = \frac{Y}{|\Sigma|_{\mathbf{y}}}P^{(1)} + \mu^{(1)}P^{(0)} + \frac{\mathbf{D}_{\mathcal{S}}^{(1)}}{\rho_e c}\cdot\mathbf{grad}_{\mathbf{x}}^{\mathcal{S}}P^{(0)} \tag{15}$$

where $\mu^{(1)}$ and $\mathbf{D}_{\mathcal{S}}^{(1)}$ describe the response of the resonators to the boundary layer radiated and scattered (due to micro-corrugation) by the resonators:

$$\mu^{(1)} = \frac{1}{|\Sigma|_{\mathbf{y}}}\int_{\Gamma_r}\mathcal{R}_{\mathbf{y}}(-\mathrm{i}\omega a^{(1)}/c)\cdot\mathbf{n}_r\, d\Gamma_{\mathbf{y}}\ ; \quad \mathbf{D}_{\mathcal{S}}^{(1)}\cdot\mathbf{e}_i = \frac{-1}{|\Sigma|_{\mathbf{y}}}\int_{\Gamma_r}\rho_e c\mathcal{R}_{\mathbf{y}}(b_i^{(1)})\cdot\mathbf{n}_r\, d\Gamma_{\mathbf{y}} \tag{16}$$

Finally, the integration of the local boundary conditions over Γ leads to the following effective boundary conditions at $\mathcal{S}$, once the fields have been rescaled as $\mathbf{V} = \mathbf{V}^{(0)} + \epsilon\mathbf{V}^{(1)}$; $P = P^{(0)} + \epsilon P^{(1)}$; $\mu = \epsilon\mu^{(1)}$; $\mathbf{D}_{\mathcal{S}} = \epsilon\mathbf{D}_{\mathcal{S}}^{(1)}$; $\mathbf{A}_{\mathcal{S}} = \epsilon\mathbf{A}_{\mathcal{S}}^{(1)}$ and $\mathbb{B}_{\mathcal{S}} = \epsilon\mathbb{B}_{\mathcal{S}}^{(1)}$:

$$\mathbf{V}\cdot\mathbf{n} = -\left(\Upsilon - \mu\right)P + \frac{\mathbf{A}_{\mathcal{S}} + \mathbf{D}_{\mathcal{S}}}{\rho_e c}\cdot\mathbf{grad}_{\mathbf{x}}^{\mathcal{S}}P + \frac{\mathbb{B}_{\mathcal{S}}}{\mathrm{i}\omega\rho_e} : \mathbf{grad}_{\mathbf{x}}^{\mathcal{S}}\left[\mathbf{grad}_{\mathbf{x}}^{\mathcal{S}}P\right] \tag{17}$$

Equation (17) shows that the boundary condition is non-local, i.e. the normal velocity component on the surface depends on the first and second in-plane gradient of pressure. When the resonators are replaced by rigid scatterers, $\mathbf{A}_{\mathcal{S}} = \mathbf{D}_{\mathcal{S}} = \mathbf{0}$, and the contribution from the simple gradient vanishes. Conversely the double-gradient contribution is the consequence of surface micro corrugation and vanishes when the resonant surface is flat, e.g., for resonators positioned behind a rigid panel.

4. Surface array of slotted cylinders upon rigid surface

To illustrate the effects of the boundary condition described by Eq. (17) on the sound wave, consider the resonant surface comprising of slotted cylinders arranged upon the rigid plane. The cylinders are supposed to be long, so the two dimensional problem is solved. The Cartesian coordinate system $(\mathbf{e}_1, \mathbf{e}_3)$ is used, with $\mathbf{e}_3 = \mathbf{n}$, and the origin O located at the rigid surface $\mathcal{S}$. The cylinders have the outer radius r, the opening S with the width e oriented at the angle α counted from $O\mathbf{n}$, the inner radius $r - e$, the inner duct of width e and length $d = \chi(r - e/2)$ positioned at the periphery of the cylinder, see Fig. 1(c). The centres of the cylinders are positioned at the points $(n\ell, r)$, where ℓ is the lateral period and n is an integer. The boundary Γ_r of the cylinder is assumed to be rigid, except for the opening, which, in turn, is assumed sufficiently small for the radial particle velocity v_o to be uniform over it, that is $\mathbf{v}_r\cdot\mathbf{n}_r = v_o\Pi_S$ at Γ_r, where Π_S is the gate function equal to 1 over the opening and 0 elsewhere on Γ_r. The velocity v_o is related to the mean value of the pressure p acting at its opening by $v_o = Y_S\langle p\rangle$ where $\langle p\rangle = |S|^{-1}\int_S p\, dS$ and Y_S is the admittance of the opening. The response function of the slotted cylinder and the normalised admittance $\rho_e c Y_S$ can be written:

$$\mathcal{R}_{\mathbf{y}}\left(p\right)\cdot\mathbf{n}_r = Y_S\langle p\rangle\,\Pi_S(\mathbf{y}) \quad ; \qquad \rho_e c Y_S = \frac{\mathrm{i}\sigma\omega_o\omega}{\omega_o^2 - \mathrm{i}2\xi\omega_o\omega - \omega^2} \tag{18}$$

where $\omega_o = \sqrt{K/M}$ is the slotted cylinder resonance frequency, $\xi \ll 1$ is the loss factor, $\sigma = \rho_e c|S|^2/M\omega_o$ the admittance parameter, K the resonator's modal stiffness and $M = \rho_e|S|h$ is its modal mass, with h being an effective neck length [1]. While Eq. (18) leads to the leading order admittance $\Upsilon = -Y_S|S|/|\Sigma|$, the following geometric elementary field $g = a/[\rho_e c Y_S]$ is defined. It satisfies:

$$\mathrm{div}_{\mathbf{y}}\left[\mathbf{grad}_{\mathbf{y}}\, g\right] = 0 \quad ; \qquad \mathbf{grad}_{\mathbf{y}}\, g \cdot \mathbf{n}_\Gamma = (|S|/|\Sigma|)\,\mathbf{n}\cdot\mathbf{n}_\Gamma - \Pi_S \text{ at } \Gamma; \tag{19}$$

along with the periodicity and evanescence conditions. Then, Eqs. (14), (16) and (18) lead to:

$$\mu = \rho_e c Y_S \Upsilon \mathrm{i}\omega\langle g\rangle/c \quad \text{and} \quad \mathbf{A}_{\mathcal{S}} = \rho_e c\Upsilon G\mathbf{e}_1 = -\mathbf{D}_{\mathcal{S}} = -\rho_e c\Upsilon\langle b_1\rangle\mathbf{e}_1, \tag{20}$$

where $G = |S|^{-1}\int_{\Gamma_r} g\mathbf{n}_r\cdot\mathbf{e}_1\, d\Gamma$. Hence, for the resonant surface made of a single slotted cylinder per period arranged upon the rigid surface, the flux produced by the resonators in response to the corrugation field b_1 is balanced by the macro-divergence of the BL radiation field a. As a result, the in-plane gradient term in Eq. (17) does not contribute to the effective boundary condition. Finally, since $M = \mathcal{O}(\epsilon\Upsilon)$, the following Taylor expansion can be performed:

$$\rho_e c\,(\Upsilon - \mu) = \rho_e c\Upsilon\left(1 - \frac{\mathrm{i}\omega\langle g\rangle}{c}\rho_e c Y_S\right) \approx \frac{\rho_e c\Upsilon}{1 + \frac{\mathrm{i}\omega\langle g\rangle}{c}\rho_e c Y_S} = \frac{-\mathrm{i}\eta\Omega_o\omega}{\Omega_o^2 - \mathrm{i}2\zeta\Omega_o\omega - \omega^2} \tag{21}$$

where, using Eq. (18) with $\omega_o = \sqrt{K/M}$ and $\sigma = \rho_e c|S|^2/M\omega_o$ with $M = \rho_e|S|h$:

$$\Omega_o^2 = \frac{K}{\rho_e|S|(h + \langle g\rangle)}\ ;\ \ \zeta = \xi/\sqrt{1 + \langle g\rangle/h}\ ;\ \ \eta = \frac{\sigma|S|}{|\Sigma|}/\sqrt{1 + \langle g\rangle/h}. \tag{22}$$

Hence, $\langle g\rangle$ is an apparent end correction for the array of resonators, which accounts for the mutual near-field interactions between all the resonators and the rigid surface. Due to the presence of the apparent end correction, the resonance frequency of the surface is lower than that of the single resonator in free field. Parameters η and ζ are also reduced. Nevertheless, the normalised admittance value $\rho_e c\,(\Upsilon - M)$ at the resonance frequency Ω_o remains unchanged and is equal to that $\rho_e c\Upsilon(\omega_o) = \sigma|S|/2\xi|\Sigma|$ at the leading order. Hence, if the admittance matching with air is achieved (critical coupling) according to leading order calculations, it will remain at the corrector order, but at a lower frequency.

Now, the reflection of the incident plane wave $P^I = P_0^I e^{\mathrm{i}kx_1\sin\theta - \mathrm{i}kx_3\cos\theta}$ from the resonant surface is studied, where θ is the angle of incidence counted from $\mathbf{n}$, $k = \omega/c$ is the air wavenumber, and $x_j = \mathbf{x}\cdot\mathbf{e}_j$. Due to the Descartes Law, it gives rise to the reflected wave $P^R = P_0^R e^{\mathrm{i}kx_1\sin\theta + \mathrm{i}kx_3\cos\theta}$. The effective surface condition in Eq. (17) leads to the reflection coefficient $R = P_0^R/P_0^I$ in the form:

$$R = \frac{\cos(\theta) - \beta(\omega,\theta)}{\cos(\theta) + \beta(\omega,\theta)}\ \ ;\ \ \ \beta(\omega,\theta) = \rho_e c(\Upsilon - \mu) - \mathrm{i}kB_{\mathcal{S}}\sin^2(\theta). \tag{23}$$

First, at normal incidence, $\theta = 0$, the non-local contributions to the boundary conditions vanish and the reflection coefficient tends to that of the surface with the effective normalised admittance $\rho_e c(\Upsilon - M)$. However, nonlocality becomes important at oblique and grazing incidence. If the slotted cylinders are replaced by rigid scatterers ($Y_S = 0$), then $\beta = -\mathrm{i}kB_{\mathcal{S}}\sin^2(\theta)$ is purely imaginary, which results in the perfect reflection of the wave, $|R| = 1$, with a phase shift that depends on the frequency and the angle of incidence.

To illustrate these effects, the resonant surface is now designed. First, note that the corrugation related characteristic length $B_{\mathcal{S}}$ depends only on the cylinders' radius r and the spacing ℓ between them. The cell problem for $\mathbf{b}_{\mathcal{S}} = b_1\mathbf{e}_1$ is solved numerically using the commercial software COMSOL Multiphysics and results are shown in Fig. 2(a). The dependence of $B_{\mathcal{S}}$ on r/ℓ is not monotonous and its maximum $B_{\mathcal{S}}/\ell \approx 0.24$ is reached at $2r/\ell \approx 0.68$. To emphasize the effects from roughness, this value is chosen in the design. The inset in Fig. 2(a) shows the color-map of the field b_1 when

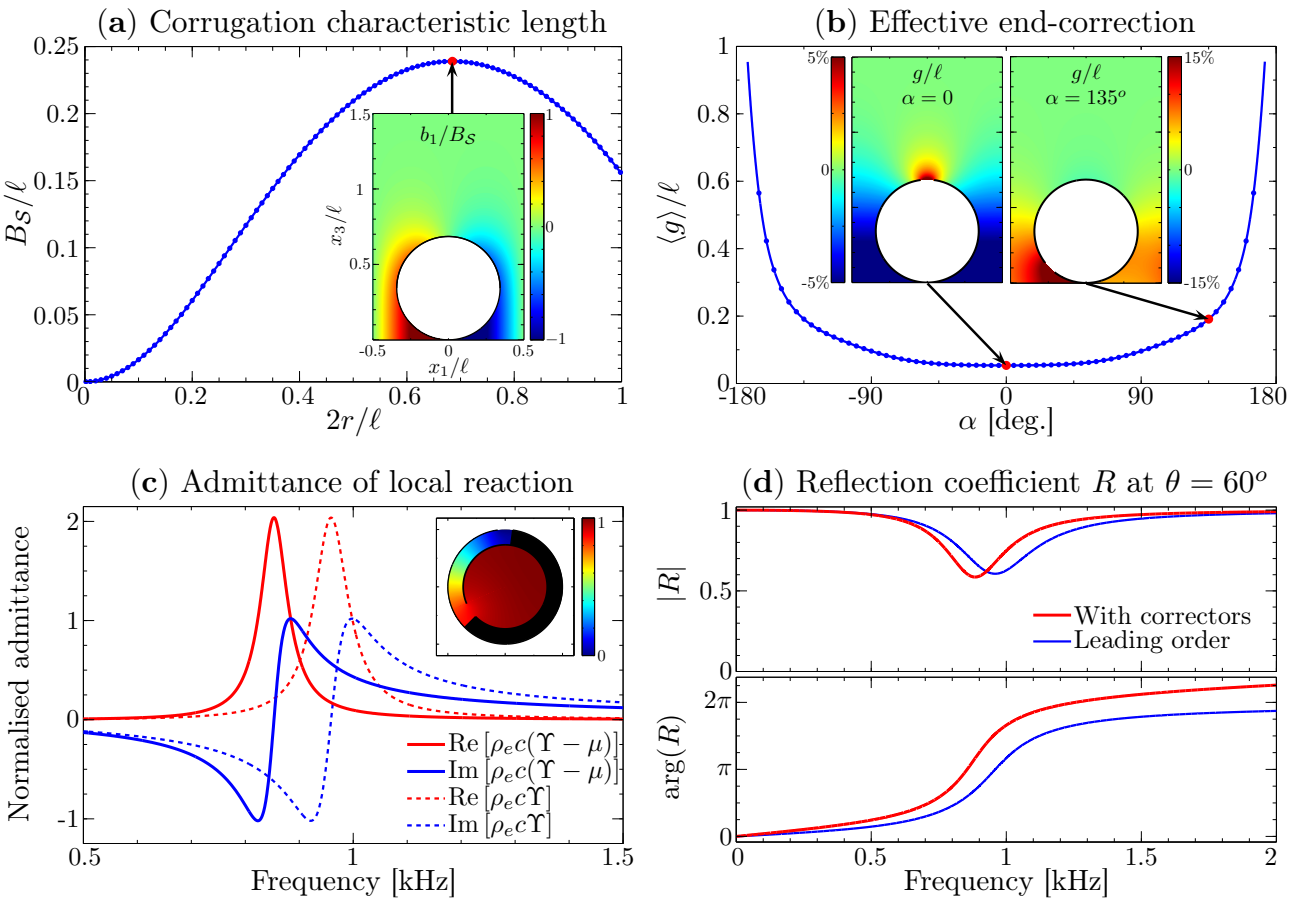

Figure 2: Behaviour of the corrugated resonant surface comprised of periodically arranged slotted cylinders with extended necks. (a) and (b) Numerical resolution of the cell problems related to the characteristic corrugation length B_S and apparent end-correction $\langle g\rangle$. (c) and (d) Comparison between the leading order and corrector order results for the effective admittance of local reaction and plane wave reflection coefficient.

B_S is at maximum. It is indeed confined to the surface, consistently with the notion of boundary layer, and nearly vanishes at $x_3 \approx \ell$. The field is antisymmetric with respect to x_1, is zero at the apex $(x_1, x_3) = (0, 2r)$ and its maximum values are attained close to the surface.

The opening angle of the slot is chosen as $e/r = 15^o$. The cell problem for g is solved numerically using COMSOL Multiphysics and results are shown in Fig. 2(b). The apparent end correction $\langle g\rangle$ is symmetric with respect to the orientation angle α. It increases with α, equal to $\langle g\rangle/\ell \approx 5.3\%$ at $\alpha = 0$, quasi-constant in the range $|\alpha| < 45^o$ with $\langle g\rangle/\ell \approx 5.8\%$ at $\alpha = 45^o$ and increases sharply for $\alpha > 45^o$. For $\alpha = 135^o$, the end correction is equal to $\langle g\rangle/\ell \approx 19\%$. The insets show the field g/ℓ at $\alpha = 0$ and $\alpha = 135^o$. It remains confined to the surface, consistently with the notion of boundary layer, and nearly vanishes at $x_3 \approx \ell$. In the following, the orientation angle $\alpha = 135^o$ is chosen.

The inner duct is now designed neglecting the inner end correction, consistently with the results from the leading order description. In that case, the resonance frequency and the admittance parameter are $\omega_o = c\sqrt{e/Vd}$ and $\sigma = \sqrt{V/de}$, with $V = \pi(r-e)^2$ being the volume of air in the inner cavity. The resonant surface is designed to achieve a scale parameter $\epsilon_o = \ell\omega_o/c \approx 0.8$ at the resonance, to emphasize the corrector contribution while keeping $\epsilon_o < 1$. That gives the angular neck length $\chi = d/r = 135^o$. The resonant surface is also designed to operate at the resonance frequency equal to 1 kHz according to the leading order description, which leads to $\ell = 4.4$ cm, $r \approx 1.5$ cm, $e \approx 4$ mm and $d \approx 3.05$ cm. To account for the inner end correction, the resonator is modelled using COMSOL Multiphysics, which gives the resonance frequency $\omega_o/2\pi = 959$ Hz and the admittance parameter

$\sigma \approx 1.8$. The modal pressure field inside the resonator is shown in Fig. 2(c). The loss factor $\xi = 4\%$ is chosen. The effective leading order admittance $\rho_e c \Upsilon$ is compared with the corrected admittance $\rho_e c\,(\Upsilon - \mu)$ in Fig. 2(c). As expected, the corrector μ leads to shift the effective admittance to lower frequencies, with the resonance frequency going down from 959 Hz to 852 Hz.

Figure 2(d) shows the reflection coefficient for the incidence angle $\theta = 60^o$ computed using either the leading order admittance or the effective surface condition accounting for the correctors. Qualitatively, both lead to: (1) sound absorption at their respective resonance frequency; and (2) a phase shift during reflection from the resonant surface. Alongside with lower resonance frequency, accounting for correctors leads to a slightly higher absorption coefficient value at resonance ($|R| \approx 0.58$ with the correctors against $|R| \approx 0.6$ at the leading order) and an additional phase shift due to corrugation, with a phase difference of about $\pi/4$ at 2 kHz.

5. Conclusion

The properties of the corrugated resonant surface have been described in terms of an effective boundary condition by means of two-scale asymptotic homogenization and boundary layer analysis. While an admittance of local reaction is found at the leading order, a non-local boundary condition is derived when the correctors are accounted for. The correctors are expected to become significant when the scale separation is poor. The model developed here has been illustrated in 2-D for the array of slotted cylinders with an extended neck, but the analytical results are valid for 3-D geometry, without any assumptions about the nature of the resonators and LW field, except for the scale separation. In particular, the non-local contribution should lead to anisotropic effects in 3-D. Further studies will concern the effects from correctors for the surface with several resonators per period and 3-D anisotropic resonators arrangement. The homogenization results will also be compared with those obtained using alternative techniques, e.g. multiple scattering theory. The results are useful for the design of corrugated resonant surfaces, where the corrugation/radiation coupling could be used to tune the resonance frequency by simply changing the positioning of the resonators. This work has been supported in part by EPSRC UK grant EP/K037234/1 and COST Action 15125 DENORMS.

REFERENCES

1. Schwan, L., Umnova, O., and Boutin, C., Sound absorption and reflection from a resonant metasurface: Homogenisation model with experimental validation, *Wave Motion*, **72**, 154–172, (2017).

2. Sanchez-Palencia, E., *Non-homogeneous media and vibration theory*, Lecture Note in Physics, vol. 127, Springer-Verlag, Berlin, (1980)

3. Auriault, J.-L., Boutin, C. , and Geindreau, C., *Homogenization of Coupled Phenomena in Heterogenous Media*, ISTE Ltd and John Wiley & Sons, Inc., (2009).

4. Boutin, C., and Roussillon, P., Wave propagation in presence of oscillators on the free surface, *Wave Motion*, **44**, 180–204, (2006). .

5. Auriault, J.-L., Borne, L., and Chambon, R., Dynamics of porous saturated media, checking of the generalized law of Darcy, *J. Acoust. Soc. Am.*, **77**(5), 1641–1650, (1985).